Report

Cell Reports

STED Nanoscopy Reveals the Ubiquity of Subcortical Cytoskeleton Periodicity in Living Neurons

Graphical Abstract

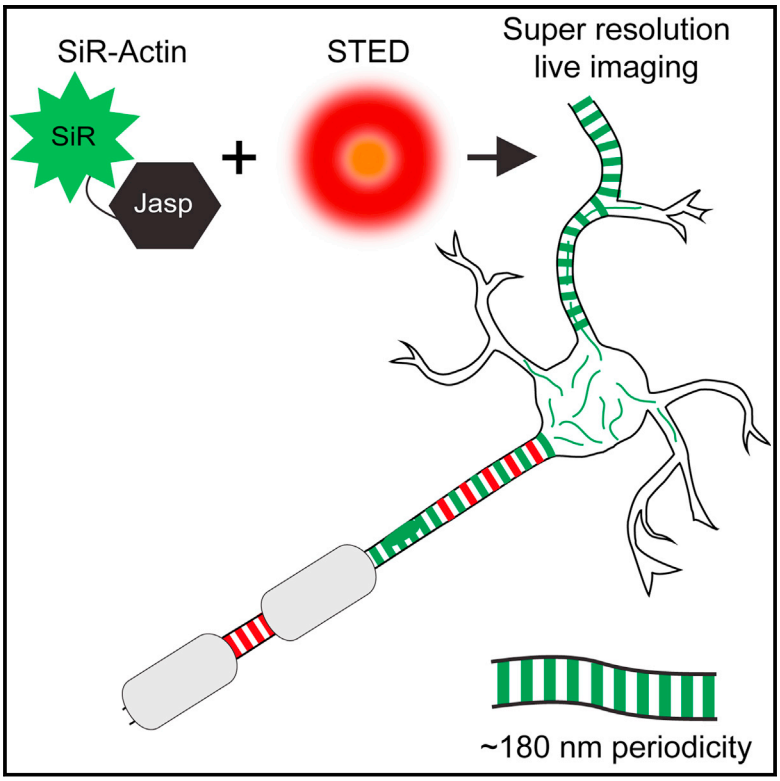

Authors

Elisa D'Este, Dirk Kamin, ...,
Ahmed El-Hady, Stefan W. Hell

Correspondence

shell@mpibpc.mpg.de

In Brief

Harnessing STED nanoscopy, D'Este et al. reveal novel patterns of actin organization at the nanoscale in living hippocampal neurons.

Highlights

- Dendrites exhibit periodic actin organization
- Cytoskeletal proteins show the same periodicity at nodes of Ranvier
- Cytosolic actin organization is developmentally and spatially regulated
- Actin patches in the axon initial segment co-localize with synaptic markers

D'Este et al., 2015, Cell Reports *10*, 1246–1251
March 3, 2015
http://dx.doi.org/10.1016/j.celrep.2015.02.007

CellPress

OPEN ACCESS
CellPress

Cell Reports
Report

STED Nanoscopy Reveals the Ubiquity of Subcortical Cytoskeleton Periodicity in Living Neurons

Elisa D'Este,[1] Dirk Kamin,[1] Fabian Göttfert,[1] Ahmed El-Hady,[1,2] and Stefan W. Hell[1,*]
[1]Department of NanoBiophotonics, Max Planck Institute for Biophysical Chemistry, Am Fassberg 11, 37077 Göttingen, Germany
[2]Present address: Princeton Neuroscience Institute, Princeton University, Princeton, NJ 08544, USA
*Correspondence: shell@mpibpc.mpg.de
http://dx.doi.org/10.1016/j.celrep.2015.02.007

SUMMARY

In the axons of cultured hippocampal neurons, actin forms various structures, including bundles, patches (involved in the preservation of neuronal polarity), and a recently reported periodic ring-like structure. Nevertheless, the overlaying organization of actin in neurons and in the axon initial segment (AIS) is still unclear, due mainly to a lack of adequate imaging methods. By harnessing live-cell stimulated emission depletion (STED) nanoscopy and the fluorescent probe SiR-Actin, we show that the periodic subcortical actin structure is in fact present in both axons and dendrites. The periodic cytoskeleton organization is also found in the peripheral nervous system, specifically at the nodes of Ranvier. The actin patches in the AIS co-localize with pre-synaptic markers. Cytosolic actin organization strongly depends on the developmental stage and subcellular localization. Altogether, the results of this study reveal unique neuronal cytoskeletal features.

INTRODUCTION

Investigations of neuronal actin organization have so far focused on structural aspects of dendritic spines (Izeddin et al., 2011; Korobova and Svitkina, 2010; Tatavarty et al., 2009; Testa et al., 2012; Urban et al., 2011; Willig et al., 2014). At the same time, very little is known about the actin architecture in axons. Recently, super-resolution fluorescence microscopy revealed a striking ring-like actin organization with a periodicity of ~180 nm in axons of cultured hippocampal neurons (Lukinavičius et al., 2014; Xu et al., 2013). Interestingly, electron microscopy failed to reveal such structural features altogether (Jones et al., 2014; Watanabe et al., 2012) and instead highlighted the presence of actin-patch features. While actin patches in axons have been identified as critical for maintaining neuronal polarity, the role of the highly periodic lattice is still unclear (Arnold and Gallo, 2014).

Disagreements regarding actin ultrastructure trace back to the fact that actin is inherently difficult to image with nanoscale resolution. This is because the actin network is too fine and too dense to be resolved by diffraction-limited optical microscopy, while the preparation required for electron microscopy is rather harsh, altering the overall structure of the network (Fifková, 1985; Schnell et al., 2012). Optical nanoscopy of phalloidin-stained actin is a good compromise between high-resolution imaging and the aggressiveness of sample preparation (Xu et al., 2012). However, it typically requires chemical fixation, which may itself cause artifacts (Schnell et al., 2012). Therefore, fluorescence nanoscopy or super-resolution of actin in living cells under relevant normal growth conditions is the method of choice for overcoming these observational limitations.

Being membrane permeable, the recently introduced silicon rhodamine actin label (SiR-Actin) allows labeling of actin inside living cells, without the need to overexpress fluorescently tagged proteins such as LifeAct, actin monomers, or actin-binding proteins. Its fluorogenicity provides a high signal-to-noise ratio, facilitating the visualization of finest details. SiR-Actin was already successfully tested for stimulated emission depletion (STED) nanoscopy, confirming the presence of a periodic actin pattern also in axons of living neurons (Lukinavičius et al., 2014). Here, we report several novel observations pertaining to subcortical actin ultrastructure, enabled by the use of SiR-Actin and two-color STED nanoscopy in living primary cultured hippocampal neurons. We discovered that subcortical actin forms a periodic structure in the dendritic compartments in addition to axonal compartments, where it is shown to appear shortly after axon specification. A similar periodic pattern of cytoskeletal proteins was also found in myelinated sciatic nerve fibers at the nodes of Ranvier. Regarding cytosolic actin in living cells, SiR-Actin reveals that its organization in patches and bundles is both evolving in time (corresponding to developmental stage) and spatially regulated (depending on subcellular compartment). Actin bundles in the somatodendritic compartment end abruptly at the beginning of the axon initial segment (AIS), while actin patches in the AIS play a role in the organization of synaptic boutons (Sankaranarayanan et al., 2003; Waites et al., 2011), since they co-localize with pre-synaptic markers. Our work reveals the ubiquity of the periodic structure of cytoskeleton in neurons and elucidates the involvement of actin in the maintenance of neuronal polarity. By the same token, our work also emphasizes the utility of live-cell nanoscopy for the study of neuronal ultrastructures, where these unprecedented imaging capabilities will undoubtedly impact the search for mechanisms that underlie basic neuronal functions.

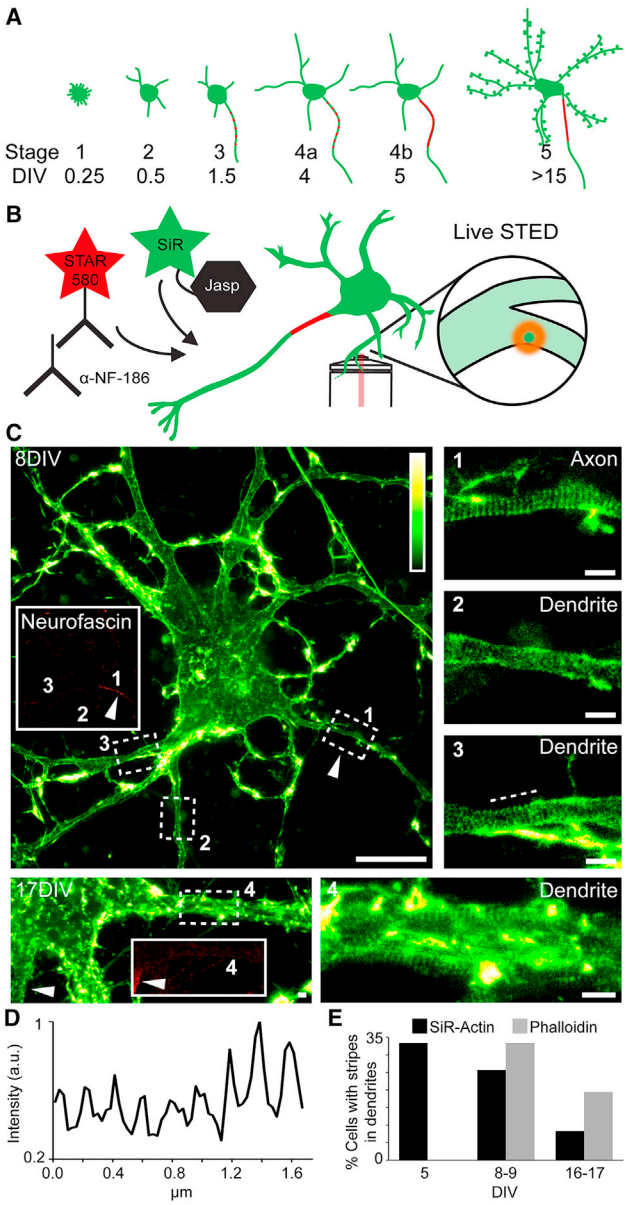

Figure 1. Live Imaging Shows a Periodic Structure of Actin Also in Neurofascin-Negative Neurites

(A) Developmental staging of neurons according to the days in vitro (DIV), axon initial segment (AIS) formation, and spine sprouting (adapted and modified from Dotti et al., 1988).

(B) Experimental procedure of live-SiR-Actin and AIS labeling for two-color STED nanoscopy. Cultured hippocampal neurons were incubated with 2 μM SiR-Actin for 1 hr under growth conditions. Afterward, the AIS was live stained with an anti-pan-neurofascin antibody (α-NF-186) to specifically mark the axon. Living neurons were then immediately imaged by two-color STED nanoscopy at room temperature.

(C) STED images of living neurons (8 and 17 DIV) in which actin periodicity is present both in the axon and also in dendrites (insets show the specific neurofascin labeling to highlight the axon). Arrowheads point to the axons. Scale bar, 10 μm for 8 DIV and 1 μm for 17 DIV. (1–4) Close-ups of the regions indicated in the images of the neurons at 8 and 17 DIV. Box 1 corresponds to the neurite positive for neurofascin (an axon), while boxes 2–4 correspond to neurites that are negative for neurofascin (dendrites). Scale bar, 1 μm.

(D) Intensity profile corresponding to the dashed line in (C) box 3.

(E) Percentage of cells in which actin periodicity can be seen also in neurofascin-negative neurites at different days in vitro, for both SiR-Actin and phalloidin stainings (SiR-Actin, three independent experiments: 5 DIV, n = 27 cells; 8–9 DIV, n = 39; 16–17 DIV, n = 24; phalloidin, two independent experiments: 5 DIV, n = 19; 8–9 DIV, n = 27; 16–17 DIV, n = 36). All images depict raw STED data. SiR-Actin is shown using a delta lookup table (LUT) and neurofascin using the fire LUT.

RESULTS

Subcortical Actin Forms a Periodic Lattice Also in Dendrites of Living Neurons

We exploited the membrane permeability of SiR-Actin to study the organization of filamentous actin (F-actin) in living neurons at different developmental stages. After 1.5 days in vitro (DIV), corresponding to developmental stage 3, cultured neurons first specify their axon, which becomes biochemically recognizable starting from 5 DIV (Dotti et al., 1988). Indeed, at this stage, the AIS assembles, and its characteristic proteins accumulate (Boiko et al., 2007) (Figure 1A). To obtain sub-diffraction resolution, we employed STED nanoscopy (Göttfert et al., 2013). Living cultured rat hippocampal neurons were first stained with SiR-Actin under growth conditions. Subsequently, the axon was identified by live labeling with an antibody directed against the extracellular domain of the AIS marker neurofascin 186 (Davis et al., 1996) (Figure 1B). This approach allowed a straightforward distinction between axons and dendrites (Figures 1C and 2). Live two-color STED imaging revealed a clear subcortical actin periodic pattern in the axons.

To our surprise, the periodic organization was readily recognizable also in neurofascin-negative processes representing dendrites (Figure 1C). The spacing of the actin lattice in dendrites was 192 ± 37 nm (n = 50) (Figure 1D) and is therefore in good agreement with the 181 ± 20 nm previously measured with STED in living axons labeled with SiR-Actin (Lukinavičius et al., 2014). This suggests that the structural arrangement of the actin scaffold is similar and likely the same in both axons and dendrites.

Next, we investigated the presence of the actin lattice in dendrites of neurons at different developmental stages in vitro, starting at 5 DIV, in order to ensure reliable distinction between axons and dendrites (Figure 1A). Overall, 90 cells between 5 and 17 DIV were analyzed using SiR-Actin labeling. An actin lattice in dendrites was visible in 21 neurons (23.3%). More specifically, the actin lattice was identified in 33.3% of neurons at 5 DIV (9 cells out of 27 imaged), 25.6% at 8–9 DIV (10 out of 39), and 8.3% at 16–17 DIV (2 out of 24) (Figure 1E). Note, however, that in neurons at >16 DIV, the presence of spines highly enriched in actin rendered the identification of the fine actin pattern much more difficult (compare Figure 1C, 17 DIV), and their presence may thus be underestimated at 16–17 DIV. Interestingly, phalloidin staining failed to identify the actin lattice in dendrites at 5 DIV, while it confirmed the results obtained with SiR-Actin labeling in cultures older than 8–9 DIV (Figures 1E and S1). While highlighting deficiencies of detection with phalloidin at early time points, this result rules out the possibility that the actin lattice is induced by the SiR-Actin dye and, at the same time, demonstrates that periodicity is not an artifact of the fixation procedure.

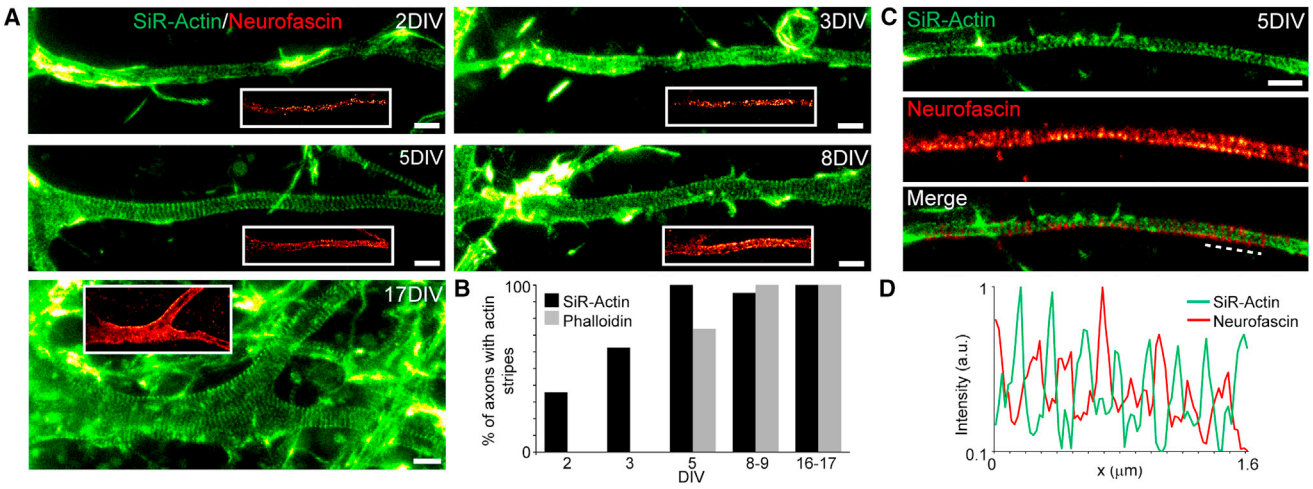

Figure 2. Actin Rings Form before AIS Specification and Intercalate with Neurofascin

(A) Representative STED images of axons of living hippocampal neurons at different days in vitro (DIV). Insets represent the specific neurofascin labeling to highlight the axon. SiR-Actin reveals that actin rings appear already at 2 DIV.

(B) Percentage of axons in which actin rings can be observed at different developmental stages, both with SiR-Actin and with phalloidin. Phalloidin has a weaker sensitivity, and actin rings could not be detected at 2–3 DIV (SiR-Actin, three independent experiments: 2 DIV, n = 28 axons; 3 DIV, n = 24; 5 DIV, n = 28; 8–9 DIV, n = 42; 16–17 DIV, n = 26; phalloidin, two independent experiments: 2 DIV, n = 20 axons; 3 DIV, n = 20; 5 DIV, n = 19; 8–9 DIV, n = 29; 16–17 DIV, n = 36).

(C) STED image of a living hippocampal neuron at 5 DIV stained with SiR-Actin (upper panel, green) and anti-neurofascin antibody (lower panel, red), and the merged image.

(D) Line profile along the dashed line in (C) showing alternating intensity peaks of actin and neurofascin.

Scale bars, 1 μm. All images depict raw STED data.

We conclude that the subcortical periodic organization of actin is not a hallmark of axons as previously reported (Xu et al., 2013) but is also present in dendrites.

The Actin Periodic Pattern Arises in Concert with Axon Specification

In fixed cells stained with phalloidin, actin rings were reported to arise in axons at around 5 DIV (Xu et al., 2013), at the time point when the AIS assembles (Figure 1A). Indeed, also in our hands, virtually all axons from 5 DIV on clearly show actin rings both with live SiR-Actin and fixed phalloidin staining (Figure 2). However, live SiR-Actin STED imaging clearly revealed the presence of actin rings in at least one of the neurites (which may develop into the axon) as early as 2–3 days before, in 35.7% of the analyzed neurons at 2 DIV, and 62.5% at 3 DIV (Figures 2A, 2B, and S2). Simultaneous two-color STED imaging revealed that neurofascin intercalates with the actin rings (Figures 2C and 2D). Note that we were not able to identify actin rings in fixed phalloidin stained neurons of 2–3 DIV (Figures 2B and S2) (Xu et al., 2013). Moreover, in some axons, both SiR-Actin and phalloidin showed a more complex lattice (Figure S2), which may provide the required rigidity when the neurite exceeds a given size.

Importantly, these results, together with the observation in dendrites, rule out the possibility that the formation of the actin pattern is dependent on AIS assembly.

The Periodic Structure of the Cytoskeleton Is Replicated at Nodes of Ranvier

So far, the periodicity of the subcortical cytoskeleton was proven only in unmyelinated cultured neurons. Yet most of the axons in the central and peripheral nervous system exhibit a myelin coat and a heterogeneous cytoskeleton with highly specialized compartments. Prominent examples include the nodes of Ranvier and the AIS. Both share a similar molecular composition of ion channels, cell-adhesion molecules, and cytoskeletal proteins (Peles and Salzer, 2000; Susuki and Rasband, 2008). One of the common cytoskeletal molecules is βIVspectrin, which was shown to exhibit ~180 nm periodicity in the AIS and is supposed to connect the actin rings (Xu et al., 2013). Therefore, we investigated the ultrastructural organization of βIVspectrin at nodes of Ranvier of mouse sciatic nerve fibers. Optical nanoscopy of myelinated axons is challenging, since the myelin sheets coating the axon generate significant aberrations. To overcome this problem, the nerve fibers were sliced into thin sections of 250–500 nm following melamine embedding (Punge et al., 2008). Unfortunately, phalloidin and SiR-Actin stainings do not persist during this procedure. The nodes were identified by co-staining CASPR (contactin-associated protein), a protein residing in the paranodal region (Einheber et al., 1997). STED nanoscopy of the sciatic nerve revealed different βIVspectrin patterns according to the relative axial position of the slice (Figure 3). A section of the middle part of the nerve (red plane in Figure 3A) shows a spotty organization of βIVspectrin only at the sides of the node (Figure 3B), with typically six to eight evenly spaced dots (Figure 3C). When a nerve was sliced at the lower or upper side (blue plane in Figure 3A), including the subcortical cytoskeletal layer, a more complex βIVspectrin pattern was observed (Figure 3D), which still exhibits ~180 nm periodicity. In total, the separation of highly resolved βIVspectrin spots at the nodes of Ranvier was on average 180 ± 35 nm (n = 49)

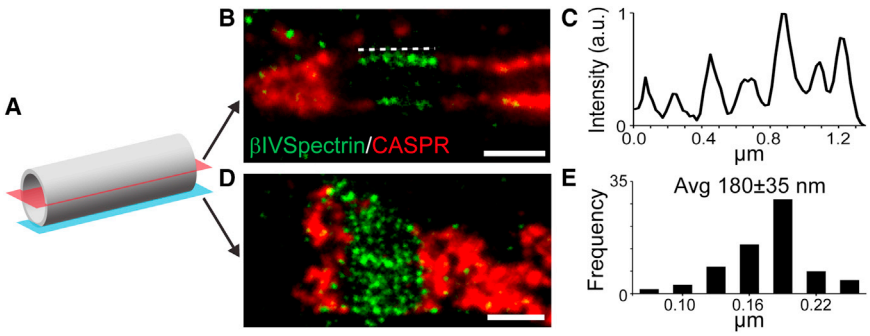

Figure 3. βIVspectrin Replicates AIS Organization at the Nodes of Ranvier

(A, B, and D) Sciatic nerves were embedded in melamine and sliced in 250–500 nm thin sections (A). Depending on the relative position of the slice to the nerve, different staining patterns can be observed. STED images of nodes of Ranvier from nerves sliced in the middle (B) or at the bottom (D). In both cases, nodes and paranodes are stained with βIVspectrin (green) and CASPR (red), respectively.

(C) Line profile along the dashed line in (B) shows ~180 nm periodicity of βIVspectrin.

(E) Distribution histogram of measured interpeak distances (n = 49 from eight nodes), indicating average spacing ± 1 SD.

Scale bars, 1 μm. Images were smoothed with a low-pass Gaussian filter.

(Figure 3E), which is in excellent agreement with the periodicity shown for the AIS of unmyelinated cultured axons. This indicates that the ultrastructural organization of the AIS is replicated at the nodes of Ranvier and demonstrates the presence of a periodicity also in sciatic nerves. Hence, the cytosolic periodic pattern may be regarded as a general, ubiquitous feature of both the central and peripheral nervous systems.

Cytosolic Actin Is Developmentally Regulated

SiR-Actin, of course, does not exclusively stain subcortical F-actin. It also stains the cytosolic F-actin pool, revealing interesting features. Focusing on axons, we noticed that the abundance of actin bundles running along the main axis varies over time, being high at 2 DIV (92.9%), decreasing until 8–9 DIV (54.2%, 39.3%, and 21.4% at 3, 5, and 8–9 DIV, respectively), and subsequently increasing again at 16–17 DIV (57.7%) (Figures 4A and 4B). In younger cultures, the filaments appear as short, not-resolvable aggregate-like objects, while in older cultures, they appear long and largely continuous and are separated well by nanoscopy (Figures 2A, 4B, and S2). In mature cultures (>16 DIV), the organization of these filaments changes dramatically at the proximal side of the AIS, forming what can be considered an actin organizational border (Figures 4B and S3). In contrast, continuity in the actin organization across somata and dendrites was observed (Figure S3). Such ultrastructural differences indeed make it possible to distinguish between axons and dendrites by using their actin organization.

Previous electron microscopy studies showed the presence of actin patches along the AIS, considering them responsible for maintaining the neuronal polarity (Arnold and Gallo, 2014; Song et al., 2009; Watanabe et al., 2012). SiR-Actin staining of living neurons highlights the presence of these patches along the AIS as well (bright localized locations in Figures 1C and 2A). Patches were seen in 52.9%, 64.5%, and 75% of axons at 5, 8–9, and 16–17 DIV, respectively, indicating a developmental increase in number (Figure S3). In order to better understand the functional significance of these patches, we analyzed whether they co-localize with the pre-synaptic active zone marker bassoon or with the synaptic vesicle marker synaptotagmin-1. In mature neuronal cultures, in which synaptic connections are already strengthened and patches are clearly visible, they co-localized with both bassoon and synaptotagmin-1 (Figures 4C and S3), indicating that they represent the scaffolds which support pre-synaptic boutons (Sankaranarayanan et al., 2003; Waites et al., 2011) rather than preventing the dendritic cargos from entering into the axon.

In conclusion, cytosolic actin organization is highly dependent on both the developmental stage of the neurons and the subcellular compartment (axonal versus somatodendritic compartment).

DISCUSSION

In this work, we used two-color STED live imaging to investigate the ultrastructure of endogenous F-actin in living cultured hippocampal neurons. Previous work showed the presence of a cytoskeletal periodic lattice as a hallmark of axons (Xu et al., 2013). SiR-Actin nanoscopy revealed the existence of the subcortical actin lattice not only in axons but also in dendrites of cultured neurons. The cytosolic actin organization is both developmentally and spatially regulated, showing diverse features at different DIV and in different subcellular compartments. We also identified a similar cytoskeletal periodic organization in nodes of Ranvier, alluding to the existence of this ultrastructural arrangement also in myelinated neurons. The use of SiR-Actin in combination with STED nanoscopy showed enhanced sensitivity compared to phalloidin staining and is thus, at present, the best way to detect fragile and fine actin features. The presented results are in agreement with an early electron microscopy study on hippocampal slices, where actin filaments were decorated with myosin S-1. There, an actin organization either in bundles or in a periodic lattice-like form was described in both dendrites and axons (Fifková and Delay, 1982). The presence of a similar cortical actin organization in both axons and dendrites may also explain how axons can acquire dendritic features when ankyrinG (the AIS master regulator) is impaired and how dendrites can turn into axons upon AIS disruption (reviewed in Rasband, 2010). Indeed, this process would require the rearrangement of cytosolic actin, but not of the subcortical actin structures. The universality of the cytoskeleton periodicity is stressed by the fact that it can be seen also at the nodes of Ranvier of sciatic nerves and hence, for the first time, in the peripheral nervous system. The organization of the cytoskeleton underneath the myelin sheet, however, still needs to be investigated.

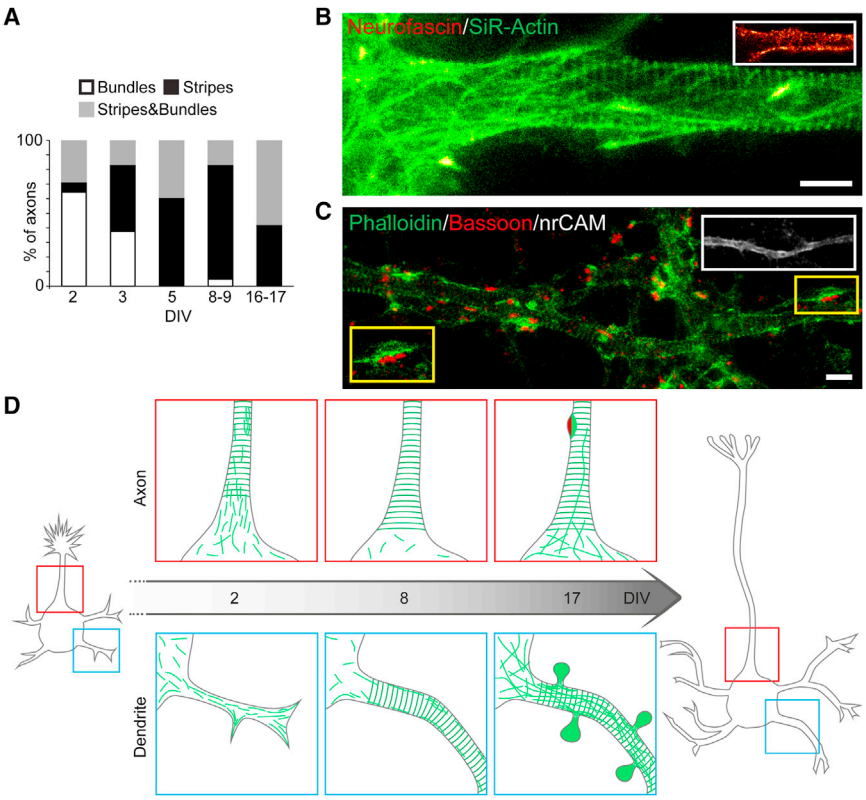

Figure 4. Cytosolic Actin Organization in Living Neurons

(A) Percentage of axons at different developmental stages in which SiR-Actin labeling shows longitudinal bundles, rings or both (same dataset as Figure 2).

(B) AIS-presenting actin filaments along the axon in living cells (24 DIV, inset shows neurofascin staining).

(C) Co-localization of actin patches (phalloidin staining, green) with bassoon (red) in fixed neurons at 17 DIV. The axon was identified by staining NrCAM (inset, white; confocal image using an Alexa-488-coupled secondary antibody). Scale bars, 1 μm. All images are raw STED data.

(D) Model of actin organization in cultured neurons at different developmental stages. The periodicity of subcortical actin in the axon is present already at 2 DIV. The cytosolic actin arrangement varies, consisting of short filaments in younger cultures (2–3 DIV) (see also Figure S2), which disappear at ~8 DIV. In mature cultures (17 DIV), long actin fibers are present, but they stop mainly at the beginning of the AIS. The red spot indicates a synaptic bouton co-localizing with an actin patch. In dendrites, the subcortical actin periodicity is not visible at 2 DIV but becomes prominent by 8 DIV, when only few actin filaments populate the dendrites. In mature cultures, the presence of spines, in which actin is highly enriched, and long filaments in the neurite make the identification of the actin periodicity less straightforward (compare Figure 1C, box 4). Note also that actin organization differs in the soma.

The functional relevance of the detected reorganizations of cytosolic actin is unclear (Figures 4A and 4D). It may link the morphological staging of neuronal development with such cytoskeletal rearrangements (Dotti et al., 1988) (Figure 1A). Actin dynamics have been implicated in long-term potentiation and can be modulated by neuronal activity (Fonseca, 2012; Ramachandran and Frey, 2009), so one may speculate that the observed cytosolic actin structures relate to neuronal plasticity.

SiR-Actin identified the presence of a cytosolic actin organizational border at the beginning of the AIS, where its organization changes dramatically. This would account for the abrupt halt of dendritic vesicles when they attempt to enter the axon (Petersen et al., 2014). Another feature of cytosolic actin is the formation of actin patches, which were thought to be the main candidates for maintaining the neuronal polarity in mature cultures (Al-Bassam et al., 2012; Arnold and Gallo, 2014; Jones et al., 2014; Song et al., 2009; Watanabe et al., 2012) or precursors of filopodia in developing sensory neurons (Spillane et al., 2011). The reported data indicate that such actin patches are the scaffolds that sustain synaptic boutons (Sankaranarayanan et al., 2003; Waites et al., 2011). Cytosolic actin seems to be involved in the maintenance of neuronal polarity, concretely, as shown here, in that its organization changes dramatically at the proximal part of the AIS. However, other unknown mechanisms or structures could be involved in the separation of the axonal from the somatodendritic compartment.

In conclusion, a number of new features below the diffraction resolution limit have been discovered, opening up new questions related to how the periodic lattice forms. Our work underscores once more the power of combining specific fluorescent probes with modern super-resolution techniques. The presented results suggest new roles for cytoskeletal proteins in controlling and regulating neuronal development, function, and plasticity.

EXPERIMENTAL PROCEDURES

Cell Preparation

Living primary cultured hippocampal neurons were stained with 2 μM SiR-Actin and neurofascin 186 and imaged as previously described (Lukinavičius et al., 2014) using a two-color STED nanoscope (Göttfert et al., 2013) (see Supplemental Experimental Procedures for details).

Antibodies

Primary antibodies and phalloidin conjugates were used as follows: anti-pan-neurofascin (UC Davis/NIH NeuroMab Facility, catalog number [cat.] 75-172; 2 μg/ml), anti-βIVSpectrinSD (a kind gift of Michele Solimena; Dresden University of Technology, Dresden, Germany; 1:100 dilution), anti-NrCAM (Abcam, cat. 24344; 1:100 dilution); anti-bassoon (Synaptic Systems, cat. 141 004; 1:100 dilution), anti-Synaptotagmin-1-Atto647N (Synaptic Systems, cat. 105 311AT1; 1:50 dilution), anti-Caspr (UC Davis/NIH NeuroMab Facility, cat. 75-001; 2 μg/ml), phalloidin-STAR635 (Abberior, cat. 2-0205-002-5; 1:50 dilution), and phalloidin-Atto590 (ATTO-TEC, cat. AD 590-81; 1:50 dilution).

Secondary antibodies (all purchased from Dianova: sheep anti-mouse, cat. 515-005-003; goat-anti-rabbit, cat. 111-005-003; donkey anti-guinea pig, cat. 706-005-148) were custom labeled with the dyes STAR580, STAR635, or STAR635P (Abberior, cat. 1-0101-005-2, cat. 1-0101-002-1, and cat. 1-0101-007-6, respectively), with the exception of Alexa 488 goat anti-rabbit (Life Technologies, cat. A-11008) (see Supplemental Experimental Procedures for details).

SUPPLEMENTAL INFORMATION

Supplemental Information includes Supplemental Experimental Procedures and three figures and can be found with this article online at http://dx.doi.org/10.1016/j.celrep.2015.02.007.

AUTHOR CONTRIBUTIONS

E.D. and D.K. designed and performed the experiments. A.E.H. contributed in performing the experiments on sciatic nerves. F.G. constructed the microscope and assisted with experimental hardware. E.D. analyzed the data. E.D., D.K., F.G., and S.W.H. wrote the paper. S.W.H. and E.D. initiated and supervised the study. All authors discussed the research.

ACKNOWLEDGMENTS

We acknowledge Kai Johnsson and Grazvydas Lukinavicius for the kind gift of the SiR-Actin probe and Michele Solimena for the βIVspectrinSD antibody. We thank Steffen J. Sahl, Alf Honigman, Ilaria Testa, and Grazvydas Lukinavicius for critical readings of the manuscript. This work was supported by the Center for Nanoscale Microscopy and Molecular Physiology of the Brain (CNMPB) in Göttingen.

Received: November 29, 2014
Revised: January 6, 2015
Accepted: January 29, 2015
Published: February 26, 2015

REFERENCES

Al-Bassam, S., Xu, M., Wandless, T.J., and Arnold, D.B. (2012). Differential trafficking of transport vesicles contributes to the localization of dendritic proteins. Cell Rep. *2*, 89–100.

Arnold, D.B., and Gallo, G. (2014). Structure meets function: actin filaments and myosin motors in the axon. J. Neurochem. *129*, 213–220.

Boiko, T., Vakulenko, M., Ewers, H., Yap, C.C., Norden, C., and Winckler, B. (2007). Ankyrin-dependent and -independent mechanisms orchestrate axonal compartmentalization of L1 family members neurofascin and L1/neuron-glia cell adhesion molecule. J. Neurosci. *27*, 590–603.

Davis, J.Q., Lambert, S., and Bennett, V. (1996). Molecular composition of the node of Ranvier: identification of ankyrin-binding cell adhesion molecules neurofascin (mucin+/third FNIII domain-) and NrCAM at nodal axon segments. J. Cell Biol. *135*, 1355–1367.

Dotti, C.G., Sullivan, C.A., and Banker, G.A. (1988). The establishment of polarity by hippocampal neurons in culture. J. Neurosci. *8*, 1454–1468.

Einheber, S., Zanazzi, G., Ching, W., Scherer, S., Milner, T.A., Peles, E., and Salzer, J.L. (1997). The axonal membrane protein Caspr, a homologue of neurexin IV, is a component of the septate-like paranodal junctions that assemble during myelination. J. Cell Biol. *139*, 1495–1506.

Fifková, E. (1985). Actin in the nervous system. Brain Res. *356*, 187–215.

Fifková, E., and Delay, R.J. (1982). Cytoplasmic actin in neuronal processes as a possible mediator of synaptic plasticity. J. Cell Biol. *95*, 345–350.

Fonseca, R. (2012). Activity-dependent actin dynamics are required for the maintenance of long-term plasticity and for synaptic capture. Eur. J. Neurosci. *35*, 195–206.

Göttfert, F., Wurm, C.A., Mueller, V., Berning, S., Cordes, V.C., Honigmann, A., and Hell, S.W. (2013). Coaligned dual-channel STED nanoscopy and molecular diffusion analysis at 20 nm resolution. Biophys. J. *105*, L01–L03.

Izeddin, I., Specht, C.G., Lelek, M., Darzacq, X., Triller, A., Zimmer, C., and Dahan, M. (2011). Super-resolution dynamic imaging of dendritic spines using a low-affinity photoconvertible actin probe. PLoS ONE *6*, e15611.

Jones, S.L., Korobova, F., and Svitkina, T. (2014). Axon initial segment cytoskeleton comprises a multiprotein submembranous coat containing sparse actin filaments. J. Cell Biol. *205*, 67–81.

Korobova, F., and Svitkina, T. (2010). Molecular architecture of synaptic actin cytoskeleton in hippocampal neurons reveals a mechanism of dendritic spine morphogenesis. Mol. Biol. Cell *21*, 165–176.

Lukinavičius, G., Reymond, L., D'Este, E., Masharina, A., Göttfert, F., Ta, H., Güther, A., Fournier, M., Rizzo, S., Waldmann, H., et al. (2014). Fluorogenic probes for live-cell imaging of the cytoskeleton. Nat. Methods *11*, 731–733.

Peles, E., and Salzer, J.L. (2000). Molecular domains of myelinated axons. Curr. Opin. Neurobiol. *10*, 558–565.

Petersen, J.D., Kaech, S., and Banker, G. (2014). Selective microtubule-based transport of dendritic membrane proteins arises in concert with axon specification. J. Neurosci. *34*, 4135–4147.

Punge, A., Rizzoli, S.O., Jahn, R., Wildanger, J.D., Meyer, L., Schönle, A., Kastrup, L., and Hell, S.W. (2008). 3D reconstruction of high-resolution STED microscope images. Microsc. Res. Tech. *71*, 644–650.

Ramachandran, B., and Frey, J.U. (2009). Interfering with the actin network and its effect on long-term potentiation and synaptic tagging in hippocampal CA1 neurons in slices in vitro. J. Neurosci. *29*, 12167–12173.

Rasband, M.N. (2010). The axon initial segment and the maintenance of neuronal polarity. Nat. Rev. Neurosci. *11*, 552–562.

Sankaranarayanan, S., Atluri, P.P., and Ryan, T.A. (2003). Actin has a molecular scaffolding, not propulsive, role in presynaptic function. Nat. Neurosci. *6*, 127–135.

Schnell, U., Dijk, F., Sjollema, K.A., and Giepmans, B.N. (2012). Immunolabeling artifacts and the need for live-cell imaging. Nat. Methods *9*, 152–158.

Song, A.H., Wang, D., Chen, G., Li, Y., Luo, J., Duan, S., and Poo, M.M. (2009). A selective filter for cytoplasmic transport at the axon initial segment. Cell *136*, 1148–1160.

Spillane, M., Ketschek, A., Jones, S.L., Korobova, F., Marsick, B., Lanier, L., Svitkina, T., and Gallo, G. (2011). The actin nucleating Arp2/3 complex contributes to the formation of axonal filopodia and branches through the regulation of actin patch precursors to filopodia. Dev. Neurobiol. *71*, 747–758.

Susuki, K., and Rasband, M.N. (2008). Spectrin and ankyrin-based cytoskeletons at polarized domains in myelinated axons. Exp. Biol. Med. (Maywood) *233*, 394–400.

Tatavarty, V., Kim, E.J., Rodionov, V., and Yu, J. (2009). Investigating subspine actin dynamics in rat hippocampal neurons with super-resolution optical imaging. PLoS ONE *4*, e7724.

Testa, I., Urban, N.T., Jakobs, S., Eggeling, C., Willig, K.I., and Hell, S.W. (2012). Nanoscopy of living brain slices with low light levels. Neuron *75*, 992–1000.

Urban, N.T., Willig, K.I., Hell, S.W., and Nägerl, U.V. (2011). STED nanoscopy of actin dynamics in synapses deep inside living brain slices. Biophys. J. *101*, 1277–1284.

Waites, C.L., Leal-Ortiz, S.A., Andlauer, T.F., Sigrist, S.J., and Garner, C.C. (2011). Piccolo regulates the dynamic assembly of presynaptic F-actin. J. Neurosci. *31*, 14250–14263.

Watanabe, K., Al-Bassam, S., Miyazaki, Y., Wandless, T.J., Webster, P., and Arnold, D.B. (2012). Networks of polarized actin filaments in the axon initial segment provide a mechanism for sorting axonal and dendritic proteins. Cell Rep. *2*, 1546–1553.

Willig, K.I., Steffens, H., Gregor, C., Herholt, A., Rossner, M.J., and Hell, S.W. (2014). Nanoscopy of filamentous actin in cortical dendrites of a living mouse. Biophys. J. *106*, L01–L03.

Xu, K., Babcock, H.P., and Zhuang, X. (2012). Dual-objective STORM reveals three-dimensional filament organization in the actin cytoskeleton. Nat. Methods *9*, 185–188.

Xu, K., Zhong, G., and Zhuang, X. (2013). Actin, spectrin, and associated proteins form a periodic cytoskeletal structure in axons. Science *339*, 452–456.

Cell Reports

Supplemental Information

STED Nanoscopy Reveals the Ubiquity of Subcortical Cytoskeleton Periodicity in Living Neurons

Elisa D'Este, Dirk Kamin, Fabian Göttfert, Ahmed El-Hady, and Stefan W. Hell

Supplemental Figures

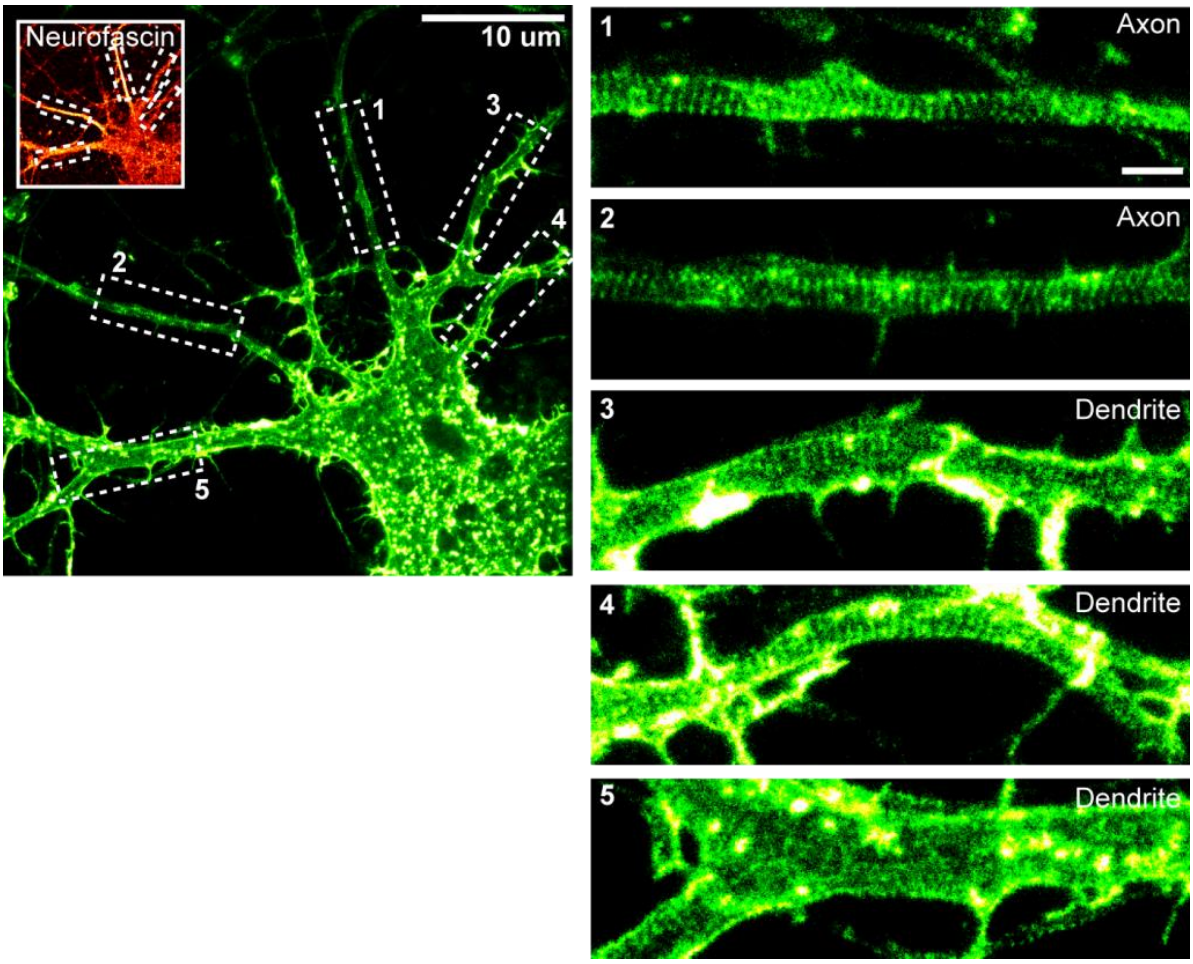

Figure S1: Phalloidin staining confirms the presence of a periodic structure of actin also in neurofascin negative neurites. Related to Figure 1. STED image of a fixed neuron at 8 DIV in which actin stripes are present also in dendrites. Neurons were stained with phalloidin-STAR635 and neurofascin (inset) to highlight the axon. Note that the neuron exhibits two axons (strong signal, inset). On the right, closeups of the boxed regions are shown. Boxes 1 and 2 correspond to neurites positive for neurofascin (i.e. axons), while boxes 3-5 correspond to neurites that are negative for neurofascin (dendrites). Scale bars 1µm. All pictures depict raw data.

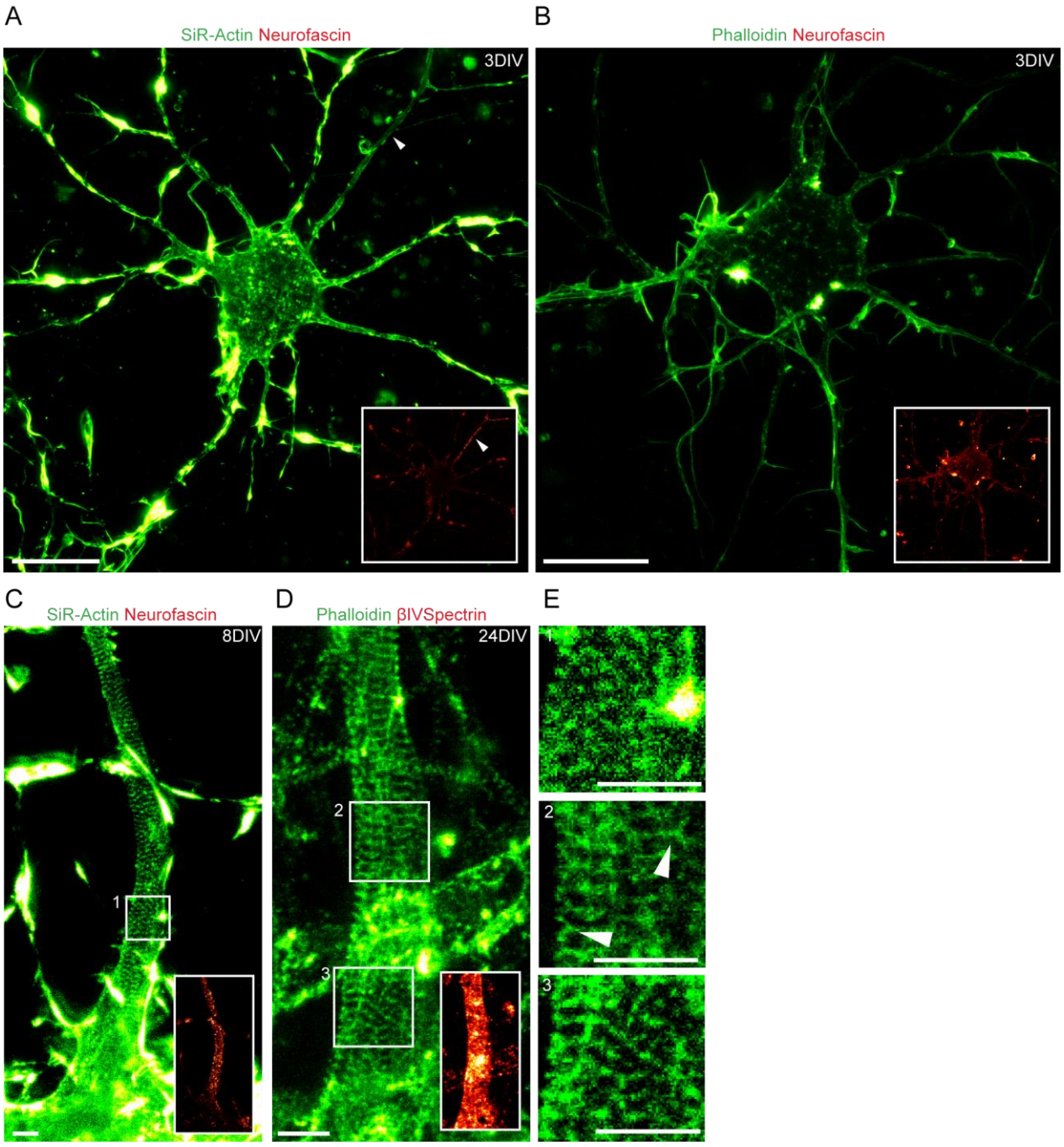

Figure S2: Features of cortical actin organization. Related to Figure 2. (A,B) Features of cortical actin organization. **(A)** STED image of a living hippocampal neuron stained with SiR-Actin (3 DIV). Inset shows the respective neurofascin staining. Arrowhead indicates a neurite enriched in neurofascin and in which an actin periodic pattern is visible (close up is shown in **Figure 2A**). **(B)** STED image of a phalloidin-stained neuron (fixed, 3 DIV). Inset shows the

respective neurofascin staining. Scale bars 10 µm. **(C, D, E)** Actin can form a more complex actin lattice. **(C)** STED image of a living hippocampal neuron stained with SiR-Actin (8 DIV). Inset shows the respective neurofascin staining to mark the AIS. SiR-Actin reveals an actin structure more complex than simple actin rings (respective box 1 in **(E)**). **(D)** STED image of a phalloidin-stained neuron (fixed, 24 DIV). Inset shows the respective βIVspectrin staining to mark the AIS. The white boxes indicate the respective enlarged regions in **(E)** (boxes 2 and 3). Like SiR-Actin, phalloidin additionally clearly reveals examples of branched filaments (arrowheads, box 2). All scale bars 1 µm. All images depict raw STED data.

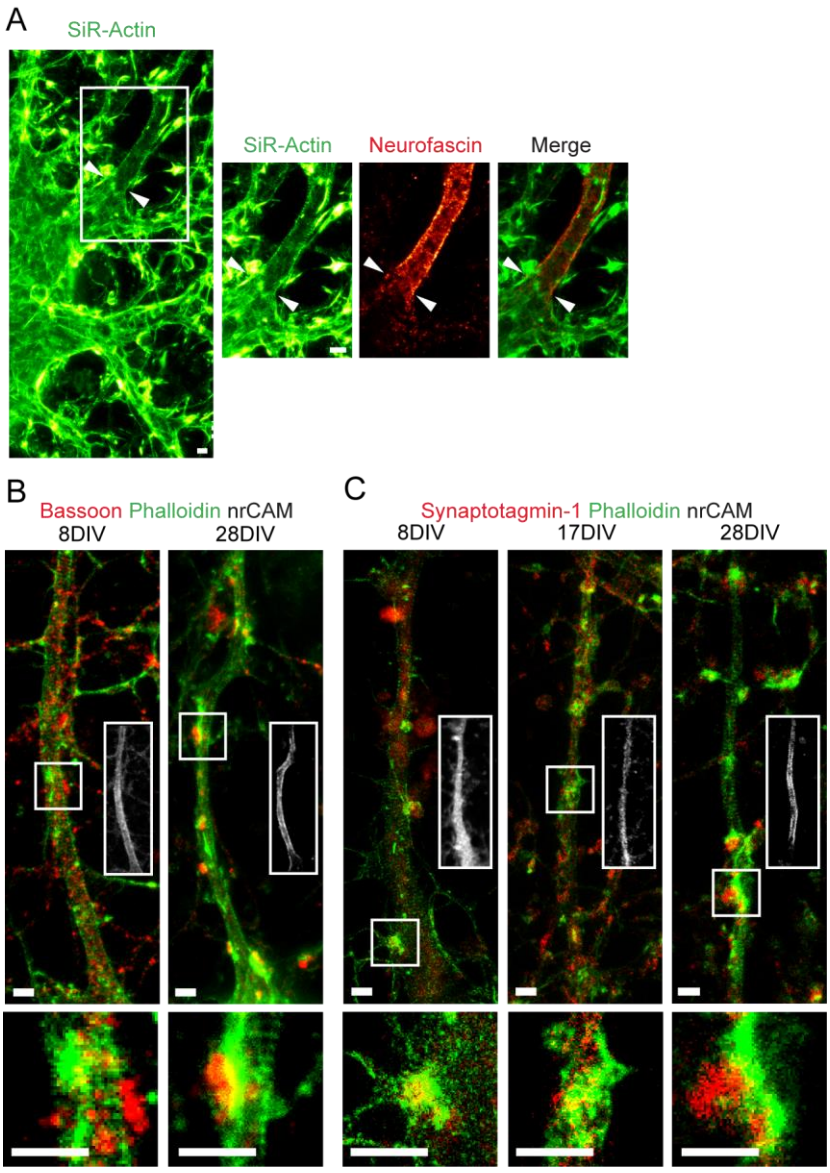

Figure S3: Features of cytosolic actin organization. Related to figure 4. (A) The cytosolic actin organizational border. STED image of both the axon (neurofascin-positive) and some dendrites of a living neuron (17 DIV). The white box indicates the respective magnified views to the right. Arrowheads indicate where neurofascin (and hence the AIS) begins. Note the difference in cytosolic actin organization between the axon and the dendrite at the bottom right of the magnified images. **(B,C)** Actin accumulates at synaptic boutons during development. **(B)** Co-localization of actin patches (phalloidin staining, green) with bassoon (red) in neurons at 8 and 28 DIV (see **Figure 4C** for 17 DIV). Axon was identified by staining NrCAM (insets, white).

(C) Same as **(B)** but with synaptotagmin-1, at 8, 17 and 28 DIV. Note that anti-synaptotagmin-1 antibody was directly coupled to Atto647N dye. Actin patches become more prominent as bassoon and synaptotagmin-1 accumulate at synaptic boutons. Scale bars 1µm. All images are raw data.

Supplemental Experimental Procedures

Primary hippocampal neuron culture preparation

Cultures of hippocampal neurons were prepared from Wistar rats of mixed sex at postnatal day P0–P1 in accordance with the regulations of the German Animal Welfare Act and under the approval of the local veterinary service. Cells were plated on coverslips coated with 100 µg/ml polyornithine (Sigma-Aldrich, cat. P3655) and 1 µg/ml laminin (BD Bioscience, cat. 354232). Neuronal cultures were maintained in Neurobasal medium (Gibco, cat. 21103049) supplemented with 2% B27 serum-free supplement (Gibco, cat. 17504044), 2 mM L-glutamine (Gibco, cat. 25030) and pen/strep (100 units/ml and 100 µg/ml, respectively, BiochromAG, cat. A2213). On the day after plating, 5 µM cytosine β-D-arabinofuranoside (Sigma, cat. C1768) was added to the cultures. Medium was replaced once per week.

Live-cell staining

Live-cell staining of actin was achieved by adding the SiR-Actin probe from a 1 mM DMSO stock solution to the growth medium at a final concentration of 2 µM. Cells were incubated for 1 h in a humidified 5% CO_2 incubator at 37°C. SiR-Actin was a kind gift of Kai Johnsson and Grazvydas Lukinavicius (both at EPFL, Lausanne, Switzerland) and is now commercially available (Spirochrome, cat. SC001).

The axon initial segment was stained for 5 min at RT with an anti–pan-neurofascin antibody (UC Davis/NIH NeuroMab Facility, cat. 75-172, 10 µg/mL), recognizing the extracellular domain of the protein, diluted in artificial cerebrospinal fluid (ACSF buffer). After three fast washes with ACSF, cells were incubated for 30 s with STAR580 (Abberior, cat. 1-0101-005-2)-labeled sheep anti-mouse secondary antibody (Dianova, cat. 515-005-003). After washing, cells were imaged in ACSF buffer at RT.

Immunostaining

Cells were washed with PBS and fixed in 4% PFA in PBS (pH 7.4) for 20 min at RT, quenched with NH_4Cl and glycine (100 mM each) for 5 min and permeabilized with 0.1% Triton X-100 for another 5 min. Both primary and secondary antibody and phalloidin incubations were performed in PBS for 1 h at RT or overnight at 4°C. Samples were mounted in Mowiol supplemented with DABCO. Incubations with phalloidin and anti-synaptotagmin-1-Atto647N antibody were performed together with the secondary antibodies.

Sciatic nerve preparation

Sciatic nerves were extracted from 3-4 months old C57BL/6 mice (both sexes), teased and frozen at -20°C on a coverslide. Samples were then fixed in ice cold methanol (-20°C) on ice for 10 min, permeabilized with 0.5% Triton X-100 in PBS for 45 min and re-equilibrated in PBS containing 0.05% Triton X-100. Both primary and secondary antibody incubations were performed for 1 h at RT in PBS supplemented with 0.05% Triton X-100. After each step, samples were rinsed 3 times for 10 min with 0.05% Triton X-100.

Samples were afterwards embedded in melamine as described before (Punge et al., 2008), following a controlled temperature regime (24 h at RT, 24 h at 40°C and 48 h at 60°C). After complete polymerization, sections of 250-500 nm thickness were cut using an ultramicrotome (EM UC6, Leica Microsystems, Wetzlar, Germany).

STED microscope

The images were obtained with a STED nanoscope described previously (Göttfert et al., 2013). Excitation of the fluorophores was performed with two pulsed diode lasers emitting ≈70 ps pulses, one at 595 nm, the other at 640 nm (both from PicoQuant, Berlin, Germany). To increase spatial resolution beyond the diffraction limit, we manipulated the beam of a pulsed, 775-nm-wavelength fiber laser (IPG Photonics) so that the focal intensity distribution exhibited a

central intensity of ~0, while the increasing intensity switches off the fluorescence ability of fluorophores surrounding the very focus center by stimulated emission. The result is a subdiffraction-sized probing area for confocal laser scanning STED nanoscopy. Using pulse energies of 3 nJ, we achieved resolutions of 30-40 nm. The excitation and STED beams were co-aligned and coupled into a 1.4 numerical aperture oil immersion lens (NA 1.4 HCX PL APO, 100x, Leica Microsystems). Sample fluorescence was collected by the same lens, spectrally separated and filtered into two ranges: 600-640 nm and 660-720 nm. The images were acquired by scanning the sample with a piezo stage (Mad City Labs) and detecting the fluorescence with an avalanche photodiode (Micro Photon Devices). A conventional confocal (i.e., diffraction-limited resolution) channel with 470 nm excitation and 500-550 nm detection wavelengths was implemented to additionally image Alexa488. The overlay of the STED and confocal channels was adjusted and verified on 100 nm TetraSpeck fluorescent beads (Life Technologies).

Processing and visualization of acquired images.

All acquired or reconstructed images were processed and visualized using ImSpector software (Max-Planck Innovation) and ImageJ (imagej.nih.gov/ij/). For visualization of the images, the “fire” and “delta” lookup tables (LUTs) of ImSpector were used. Brightness and contrast were linearly adjusted for the entire images. Line profiles were measured with ImageJ software along a 3-5 pixel wide line (for cultured neurons) or a 5-15 pixel wide line (for nodes of Ranvier). Interpeak distances were determined using the multi-peak fitting function in OriginPro8.5.